

MerTK receptor cleavage promotes plaque necrosis and defective resolution in atherosclerosis

Bishuang Cai,¹ Edward B. Thorp,² Amanda C. Doran,¹ Brian E. Sansbury,³ Mat J.A.P. Daemen,⁴ Bernhard Dorweiler,⁵ Matthew Spite,³ Gabrielle Fredman,⁶ and Ira Tabas^{1,7}

¹Department of Medicine, Columbia University, New York, New York, USA. ²Department of Pathology, Feinberg Cardiovascular Research Institute, Northwestern University, Chicago, Illinois, USA.

³Center for Experimental Therapeutics and Reperfusion Injury, Brigham and Women's Hospital and Harvard Medical School, Boston, Massachusetts, USA. ⁴Academic Medical Center, Department of Pathology, Cardiovascular Research, Amsterdam, Netherlands. ⁵Department of Cardiothoracic and Vascular Surgery, Universitätsmedizin Mainz, Mainz, Germany. ⁶Department of Molecular and Cellular Physiology, Center for Cardiovascular Sciences, Albany Medical College, Albany, New York, USA. ⁷Department of Pathology and Cell Biology and Department of Physiology, Columbia University, New York, New York, USA.

Atherothrombotic vascular disease is often triggered by a distinct type of atherosclerotic lesion that displays features of impaired inflammation resolution, notably a necrotic core and thinning of a protective fibrous cap that overlies the core. A key cause of plaque necrosis is defective clearance of apoptotic cells, or efferocytosis, by lesional macrophages, but the mechanisms underlying defective efferocytosis and its possible links to impaired resolution in atherosclerosis are incompletely understood. Here, we provide evidence that proteolytic cleavage of the macrophage efferocytosis receptor c-Mer tyrosine kinase (MerTK) reduces efferocytosis and promotes plaque necrosis and defective resolution. In human carotid plaques, MerTK cleavage correlated with plaque necrosis and the presence of ischemic symptoms. Moreover, in fat-fed LDL receptor-deficient (*Ldlr*^{-/-}) mice whose myeloid cells expressed a cleavage-resistant variant of MerTK, atherosclerotic lesions exhibited higher macrophage MerTK, lower levels of the cleavage product soluble Mer, improved efferocytosis, smaller necrotic cores, thicker fibrous caps, and increased ratio of proresolving versus proinflammatory lipid mediators. These findings provide a plausible molecular-cellular mechanism that contributes to defective efferocytosis, plaque necrosis, and impaired resolution during the progression of atherosclerosis.

Introduction

Atherothrombotic vascular disease is the leading cause of death in the industrialized world. While the majority of atherosclerotic lesions are clinically silent, acute cardiovascular events can be triggered by lesions with plaque necrosis, thin collagenous “caps” covering necrotic cores, and increased inflammation (1). We and others have highlighted the role of 2 processes: defective efferocytosis, which leads to postapoptotic necrosis; and an impaired inflammation resolution response, which contributes to persistent plaque inflammation, fibrous cap thinning, and thrombosis (2–5). Interestingly, efferocytosis has been linked to resolution of inflammation (6–8), which suggested to us an integrated pathophysiological hub in the formation of clinically dangerous plaques.

Here we focus on a macrophage efferocytosis receptor called c-Mer tyrosine kinase (MerTK), which mediates efferocytosis in atherosclerotic lesions (9, 10), has been linked to resolution (8), and can be cleaved by ADAM17 (8, 11, 12). Moreover, macrophages near the necrotic core of human atheromas were shown to have lower MerTK and higher ADAM17 than peripheral lesional macrophages (13). In this context, we hypothesized that MerTK cleavage promotes defective efferocytosis and impaired resolution in atherosclerosis.

Conflict of interest: The authors have declared that no conflict of interest exists.

Submitted: September 2, 2016; **Accepted:** November 22, 2016.

Reference information: *J Clin Invest*. 2017;127(2):564–568.

<https://doi.org/10.1172/JCI90520>.

Results and Discussion

We analyzed cross sections of carotid artery endarterectomy specimens from 14 patients for soluble Mer (sol-Mer), a marker of MerTK cleavage (11, 12), and plaque necrosis and found that lesional sol-Mer was positively correlated with necrosis (Figure 1A and Supplemental Figure 1A; supplemental material available online with this article; doi:10.1172/JCI90520DS1). Sol-Mer was not detected in nonatherosclerotic human arteries. We next compared carotid plaques from additional subjects who either had suffered a transient ischemic attack or stroke (symptomatic) or were asymptomatic. Plaques of symptomatic patients had higher levels of sol-Mer compared with those of asymptomatic patients (Figure 1B), and plasma sol-Mer was also increased in symptomatic patients (Supplemental Figure 1B).

MerTK cleavage causes defective MerTK-mediated efferocytosis (8, 11, 12). A previous study showed that recombinant sol-Mer can inhibit efferocytosis in vitro, presumably through competition for molecules that bridge apoptotic cells (ACs) to MerTK, like GAS6 (11). However, we found that recombinant sol-Mer inhibited efferocytosis only at doses that were more than 1,000-fold those in plasma (Supplemental Figure 1C). Thus, unless sol-Mer concentrations in lesions reach extremely high levels, sol-Mer is most likely a marker rather than a cause of defective MerTK efferocytosis. In this context, we found that cell-surface MerTK in macrophage-rich areas in plaques from symptomatic patients was less than that in asymptomatic patients (Figure 1C) despite sim-

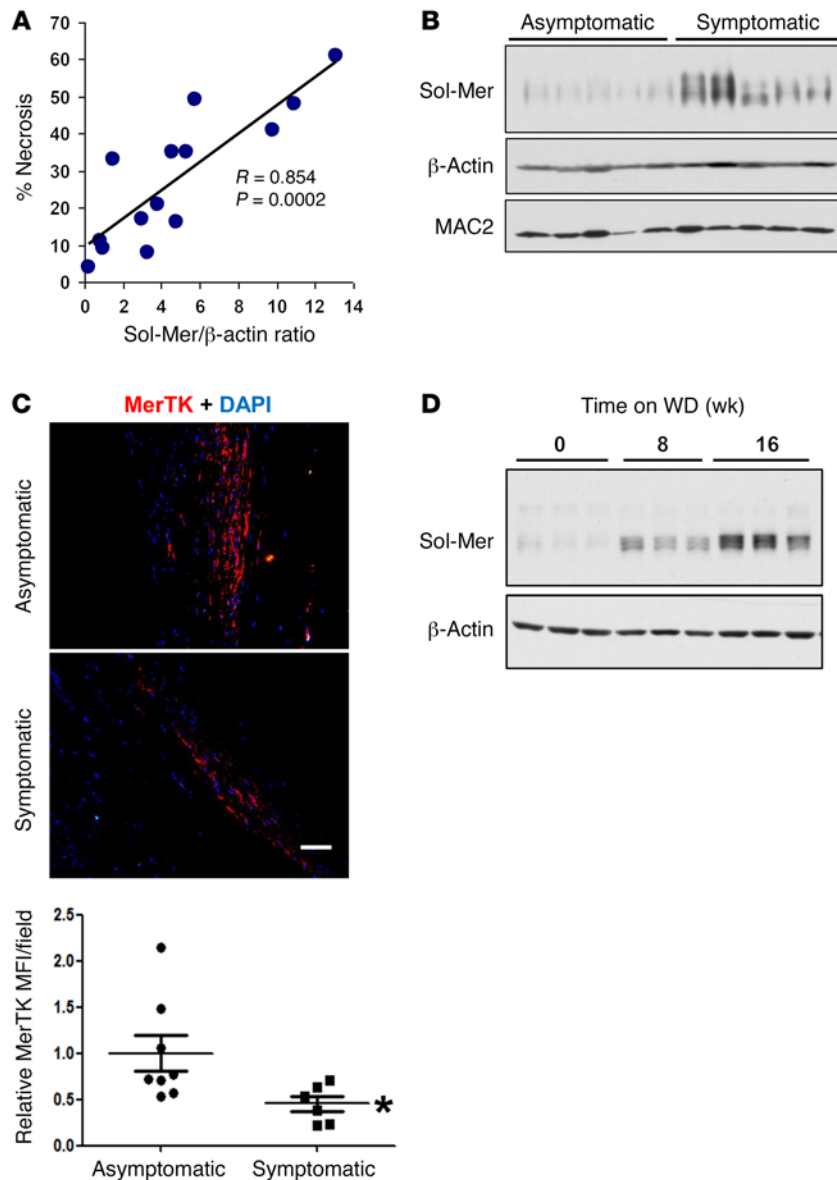


Figure 1. Sol-Mer is increased in advanced human and murine atherosclerotic lesions. (A) Carotid endarterectomy (CEA) specimens were analyzed for sol-Mer by immunoblot, and necrotic area was measured from H&E-stained images. The correlation coefficient (R) and P value were based on Pearson's product-moment correlation analysis. (B) CEA specimens from asymptomatic and symptomatic patients were assessed by immunoblot for sol-Mer ($n = 5$ per group). β -Actin and MAC2 were used as loading controls for total protein and macrophages, respectively. (C) Paraffin-embedded CEA sections were stained with anti-MerTK antibody, imaged by confocal microscopy (scale bar: 30 μ m), and quantified by MerTK mean fluorescence intensity (MFI) relative to the asymptomatic cohort ($n = 6$ –8 for each group). * $P < 0.05$, by 2-tailed Student's t test. (D) Age-matched *Ldlr*^{-/-} mice were fed the Western-type diet (WD) for 0, 8, or 16 weeks and sacrificed at 24 weeks of age. The aortic arch, Brachiocephalic Artery (BCA), and descending aorta up to the renal bifurcation were removed en bloc and immunoblotted for sol-Mer ($n = 3$ per group).

To study advanced atherosclerosis, WT or *Mertk*^{CR} bone marrow was transplanted into *Ldlr*^{-/-} mice, and atherosclerotic lesions and plasma were analyzed after 16 weeks of WD feeding. These 2 groups had similar body weight, blood glucose, plasma lipids, and circulating leukocytes (Supplemental Figures 3 and 4). We confirmed that aortic sol-Mer was reduced and that MerTK was higher in the CR cohort (Figure 2, A and B). Most importantly, *Mertk*^{CR} lesions had substantially less plaque necrosis but no change in total lesion area or lesional cell composition (Figure 2C and Supplemental Figure 5), indicating a true decrease in percentage necrosis. Further, *Mertk*^{CR} lesions had a markedly lower ratio of free to macrophage-associated TUNEL⁺ (apoptotic) cells (Figure 2D), which reflects improved efferocytosis.

Mertk^{CR} lesions also had thicker fibrous cap thickness and increased collagen gene expression (Figure 3, A and B), which are associated with plaque stability and inflammation resolution (1, 15). These lesions also had more Tregs (Figure 3C), which can promote resolution (16, 17), are decreased in human and mouse advanced atheroma (18), and have been causatively linked to plaque progression in mice (19).

Defective inflammation resolution can be caused by an imbalance between specialized proresolving mediators (SPMs) and proinflammatory lipid mediators in both human and mouse lesions (20, 21). Using liquid chromatography–tandem mass spectrometry to assay a wide range of SPMs and proinflammatory lipid mediators in aortic extracts, we found that the global content of SPMs, including resolvin D2, D5, and E3, was significantly increased in *Mertk*^{CR} extracts (Supplemental Table 1 and Figure 3D).

The inflammation resolution program has a number of positive-feedback processes. First, SPMs can increase production of proteins that dampen inflammation and promote repair (22, 23).

ilar macrophage content (Supplemental Figure 1D). Finally, aortic sol-Mer in LDL receptor-deficient (*Ldlr*^{-/-}) mice increased as a function of time on Western-type diet (WD) (Figure 1D), which correlates with plaque progression (14).

To test the hypothesis that MerTK cleavage promotes plaque necrosis, we used a mouse model in which endogenous *Mertk* was replaced with a genetically engineered mutant gene encoding cleavage-resistant MerTK (*Mertk*^{CR}) (8). Cleavage-resistant MerTK is functional under basal conditions but, unlike WT MerTK, maintains full activity under cleavage-promoting conditions, e.g., in the presence of inflammatory stimuli (8). We show here that the atherogenic lipoprotein oxidized LDL (oxLDL) increased sol-Mer and decreased cell-surface MerTK in control (WT) macrophages but not in macrophages pretreated with the ADAM17 inhibitor TAPI-0 (Supplemental Figure 2A) or in macrophages isolated from *Mertk*^{CR} mice (Supplemental Figure 2, B and C). Importantly, oxLDL suppressed efferocytosis in WT but not *Mertk*^{CR} macrophages (Supplemental Figure 2D).

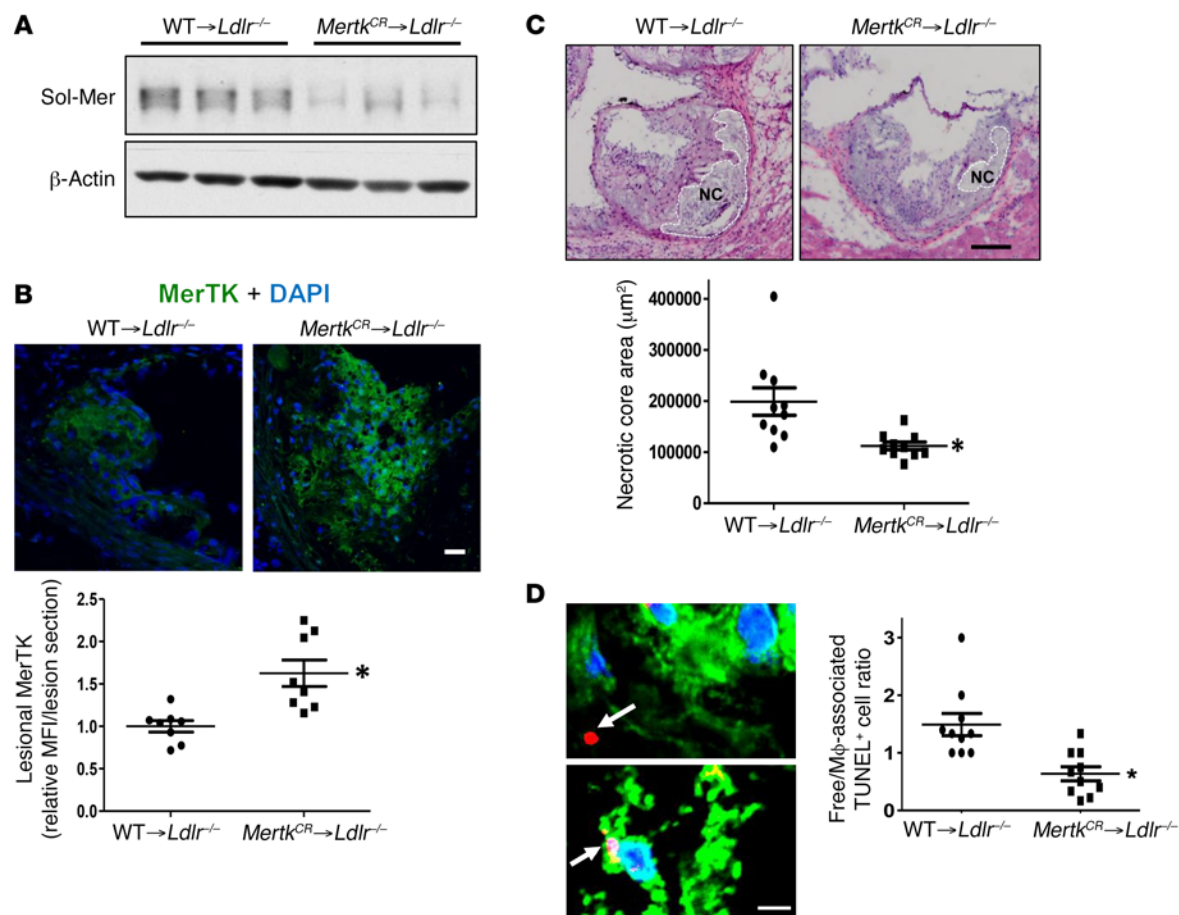


Figure 2. Suppression of MerTK cleavage in myeloid cells improves efferocytosis and decreases plaque necrosis in WD-fed *Ldlr*^{-/-} mice. (A) WT \rightarrow *Ldlr*^{-/-} or *Mertk*^{CR} \rightarrow *Ldlr*^{-/-} bone marrow-transplanted mice were fed WD for 16 weeks. Aortas were harvested and analyzed for sol-Mer as described in Figure 1D ($n = 3$ per group). * $P < 0.05$. (B) Confocal microscopy of MerTK in aortic root cross sections (scale bar: 20 μ m). Images were quantified as MerTK MFI relative to the WT \rightarrow *Ldlr*^{-/-} cohort ($n = 8$ per group). * $P < 0.01$. (C) Representative H&E images of aortic root sections, with necrotic core (NC) regions indicated by broken lines (scale bar: 40 μ m), and quantification of necrotic core area ($n = 10$ per group, 2 independent experiments). * $P < 0.01$. (D) Representative images of aortic root sections in which apoptotic cells were labeled by TUNEL (red), macrophages by anti-F4/80 (green), and nuclei by Hoechst (blue) (scale bar: 10 μ m). The white arrows depict apoptotic cells that were either free (top image) or associated with macrophages (bottom image). The graph shows quantification of the ratio of free to macrophage-associated apoptotic cells ($n = 10$ for each group, 2 independent experiments). * $P < 0.05$. A 2-tailed Student's *t* test was used for all panels.

Two such proteins, TGF- β 1 and IL-10, were significantly increased in *Mertk*^{CR} plasma (Supplemental Figure 6A). Second, SPMs can upregulate their own receptors (24), and we found that the expression of the SPM receptor ALX/FPR2 was markedly induced in the lesions of *Mertk*^{CR} mice (Supplemental Figure 6B). Third, engagement of MerTK by apoptotic cells and other ligands in cultured macrophages and in sterile inflammation *in vivo* enhances the synthesis of 5-LOX-derived SPMs at the expense of inflammatory leukotrienes (8, 25). We therefore analyzed the ratio of 5-LOX-derived SPMs to leukotrienes and found that this ratio was markedly increased in *Mertk*^{CR} extracts (Figure 3E). Moreover, this ratio was negatively correlated with necrotic core area (Figure 3F). Fourth, using bone marrow-derived macrophages, we found that resolvin D1 (RvD1) blocks LPS-induced MerTK cleavage (Supplemental Figure 7, A and B). Importantly, when WD-fed *Ldlr*^{-/-} mice were treated with RvD1, which suppresses plaque necrosis and improves lesional efferocytosis (20), lesional MerTK expression was increased (Supplemental Figure 7C). Thus, MerTK cleavage during plaque progression suppresses the integrated processes of

efferocytosis and inflammation resolution and disrupts several components of positive-feedback signaling. These findings likely explain the marked improvement in plaque morphology in the atherosclerotic lesions of *Mertk*^{CR} \rightarrow *Ldlr*^{-/-} mice.

Understanding processes involved in the formation of the unique types of atherosclerotic plaques that cause acute cardiovascular events is a critical goal in cardiovascular research. Progression to plaque necrosis is a key process because of the highly inflammatory and plaque-destabilizing nature of the necrotic core (26). Data from human and mouse studies suggest that plaque necrosis results from 2 complementary processes, postapoptotic necrosis secondary to defective efferocytosis as examined here (2, 3) and a primary cell necrosis process called necroptosis (27, 28). While the current study is focused on an efferocytosis defect in phagocytes themselves, a recent study showed that some apoptotic cells in human and mouse lesions inappropriately retain CD47, which blocks their engulfment by normal phagocytes (29). Interestingly, oxLDL, which was shown here to promote MerTK cleavage and defective efferocytosis, can induce necroptosis in macrophages, and these cells are also poorly

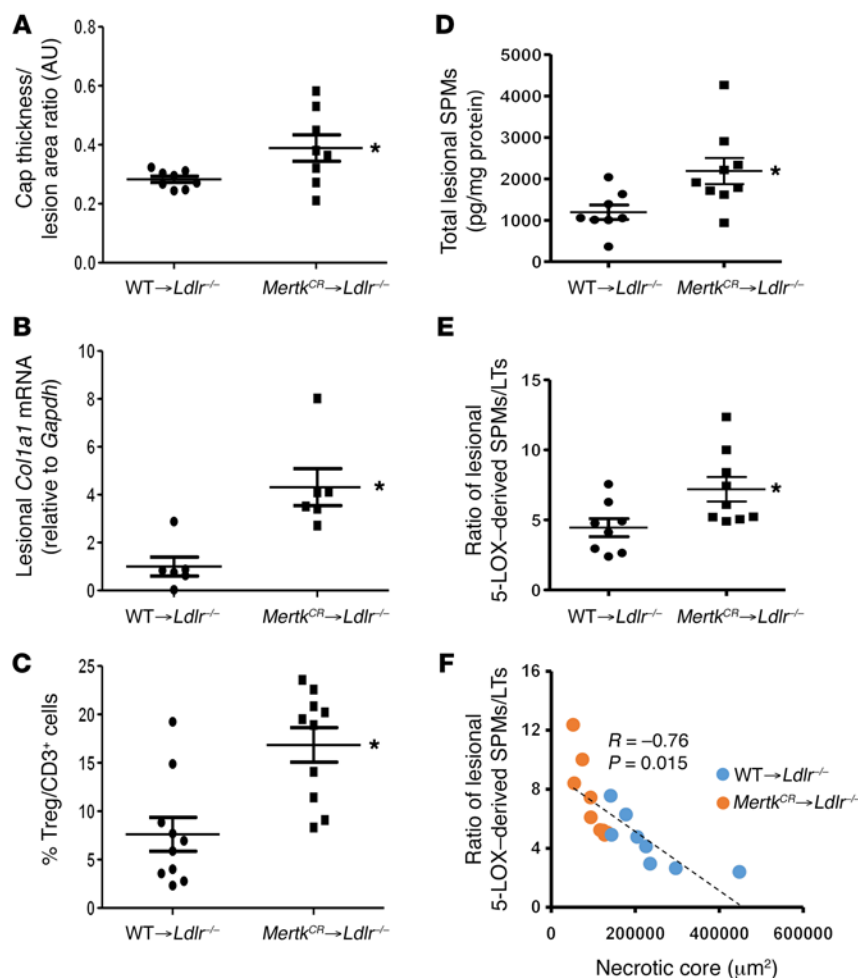


Figure 3. Suppression of MerTK cleavage improves features of resolution in plaques and increases aortic content of specialized proresolving mediators. (A) Aortic root sections from WT → *Ldlr*^{-/-} and *Mertk*^{CR} → *Ldlr*^{-/-} bone marrow-transplanted mice were stained with Picrosirius red. Quantified data are presented as the ratio of fibrous cap thickness to lesion area, expressed as arbitrary units (AU) ($n = 8$ per group). $*P < 0.05$. (B) A subset of aortic root sections was chosen randomly for quantification of *Col1a1* mRNA by reverse transcriptase quantitative PCR, with normalization to *Gapdh* mRNA ($n = 6$ for each group). $*P < 0.05$. (C) FoxP3⁺ Tregs and total CD3⁺ T cells were quantified in aortic root sections by immunofluorescence microscopy and expressed as percentage Tregs/CD3⁺ cells ($n = 10$ for each group). The average absolute numbers of these cells, most of which were in the adventitia, were 8 ± 2.49 and 19 ± 3.74 per section for FoxP3⁺ Tregs ($*P < 0.05$) and 106 ± 16.13 and 107 ± 14.33 per section for CD3⁺ cells (NS) for the WT and *Mertk*^{CR} cohorts, respectively. (D and E) Quantification of specialized proresolving mediators (SPMs) and ratio of aortic 5-LOX-derived SPMs/leukotrienes (LTs) in aorta of WT → *Ldlr*^{-/-} ($n = 8$) versus *Mertk*^{CR} → *Ldlr*^{-/-} ($n = 9$) bone marrow-transplanted mice. $*P < 0.05$. (F) Correlation of the ratio of 5-LOX-derived SPMs/leukotrienes with necrotic core area ($n = 17$). P represents the 2-tailed probability value of a Pearson correlation coefficient. A 2-tailed Student's t test was used for A–E.

internalized by normal phagocytes (28). Defects in multiple steps of efferocytosis, together with activation of necroptotic pathways in advanced plaques, would create a “perfect storm” for the development of plaque necrosis.

Our data support the concept that MerTK plays an integral part in a program of feedback signaling that amplifies resolution. This concept aligns with previous studies showing that (a) engagement of MerTK by apoptotic cells or other activators can activate both antiinflammatory and proresolving pathways (6–8, 30–32); and (b) proresolving mediators can promote MerTK expression and efferocytosis (7, 33, 34). Thus, when MerTK is rendered inactive by proteolytic cleavage, not only is there a defect in efferocytosis, but positive-feedback signaling in resolution is impaired, leading to loss of resolving mediators and further defects in efferocytosis. In the setting of advanced atherosclerosis, this profound deficit promotes key features of clinically dangerous plaques, including necrosis, imbalance of proresolving versus proinflammatory lipid mediators, fibrous cap thinning, and deficiency of Tregs. The finding that cleavage of a single molecule in the setting of a chronic inflammatory condition could have such robust pathophysiological effects not only suggests its potential as a therapeutic target but also raises the question of the possible role of MerTK cleavage in other chronic inflammatory conditions previously linked to MerTK and sol-Mer, e.g., systemic lupus erythematosus and Sjögren's syndrome (35–38).

Methods

A complete description of methods is provided in the Supplemental Methods.

Statistics. Data are displayed as mean \pm SEM. Because all data in this study fit a normal distribution, a 2-tailed Student's t test was used to determine statistical significance. P values less than 0.05 were considered significant. For the data in Figure 1A, correlation coefficient (R) and P value were calculated using Pearson product-moment correlation analysis.

Study approval. For human studies, carotid endarterectomy samples were obtained from M.J.A.P. Daemen, Academic Medical Center, Amsterdam, the Netherlands, and Bernhard Dorweiler, University Medical Center, Johannes-Gutenberg University, Mainz, Germany. Use of all material conformed with the declaration of Helsinki and was approved by the appropriate university ethics review board. Complete details are available in the Supplemental Methods. All animals were cared for according to NIH and IACUC guidelines in a barrier facility at Columbia University Medical Center, New York, New York, USA.

Author contributions

BC, EBT, GF, and IT conceived and designed the research. MJAPD and BD donated patient samples and were instrumental in the interpretation of the human data. BC, EBT, BES, MS, and GF conducted the experiments. BC, EBT, ACD, BES, GF, MS, and IT analyzed the data. BC, ACD, and IT wrote the paper.

Acknowledgments

We thank Ying Wang for assistance with the bone marrow transplantation experiments. This work was supported by an American Heart Association postdoctoral fellowship (to BC), NIH grant T32 HL007854-21 (to ACD), NIH R00 grant HL119587 (to GF), American Federation for Aging Research grant A16034

(to GF), and NIH grants HL106173 and GM095467 (to MS) and HL132412, HL075662, and HL127464 (to IT).

Address correspondence to: Ira Tabas, Columbia University, 630 W. 168th Street, New York, New York 10032, USA. Phone: 212.305.9430; E-mail: iat1@columbia.edu.

- Virmani R, Kolodgie FD, Burke AP, Farb A, Schwartz SM. Lessons from sudden coronary death: a comprehensive morphological classification scheme for atherosclerotic lesions. *Arterioscler Thromb Vasc Biol.* 2000;20(5):1262–1275.
- Schrijvers DM, De Meyer GR, Kockx MM, Herman AG, Martinet W. Phagocytosis of apoptotic cells by macrophages is impaired in atherosclerosis. *Arterioscler Thromb Vasc Biol.* 2005;25(6):1256–1261.
- Tabas I. Consequences and therapeutic implications of macrophage apoptosis in atherosclerosis: the importance of lesion stage and phagocytic efficiency. *Arterioscler Thromb Vasc Biol.* 2005;25(11):2255–2264.
- Merched AJ, Ko K, Gotlinger KH, Serhan CN, Chan L. Atherosclerosis: evidence for impairment of resolution of vascular inflammation governed by specific lipid mediators. *FASEB J.* 2008;22(10):3595–3606.
- Tabas I. Macrophage death and defective inflammation resolution in atherosclerosis. *Nat Rev Immunol.* 2010;10(1):36–46.
- Schwab JM, Chiang N, Arita M, Serhan CN. Resolvin E1 and protectin D1 activate inflammation-resolution programmes. *Nature.* 2007;447(7146):869–874.
- Mitchell S, et al. Lipoxins, aspirin-triggered epi-lipoxins, lipoxin stable analogues, and the resolution of inflammation: stimulation of macrophage phagocytosis of apoptotic neutrophils in vivo. *J Am Soc Nephrol.* 2002;13(10):2497–2507.
- Cai B, et al. MerTK cleavage limits proresolving mediator biosynthesis and exacerbates tissue inflammation. *Proc Natl Acad Sci U S A.* 2016;113(23):6526–6531.
- Thorp E, Cui D, Schrijvers DM, Kuriakose G, Tabas I. Mertk receptor mutation reduces efferocytosis efficiency and promotes apoptotic cell accumulation and plaque necrosis in atherosclerotic lesions of apoE^{-/-} mice. *Arterioscler Thromb Vasc Biol.* 2008;28(8):1421–1428.
- Ait-Oufella H, et al. Defective mer receptor tyrosine kinase signaling in bone marrow cells promotes apoptotic cell accumulation and accelerates atherosclerosis. *Arterioscler Thromb Vasc Biol.* 2008;28(8):1429–1431.
- Sather S, et al. A soluble form of the Mer receptor tyrosine kinase inhibits macrophage clearance of apoptotic cells and platelet aggregation. *Blood.* 2007;109(3):1026–1033.
- Thorp E, Vaisar T, Subramanian M, Mautner L, Blobel C, Tabas I. Shedding of the Mer tyrosine kinase receptor is mediated by ADAM17 protein through a pathway involving reactive oxygen species, protein kinase C δ , and p38 mitogen-activated protein kinase (MAPK). *J Biol Chem.* 2011;286(38):33335–33344.
- Garbin U, et al. Expansion of necrotic core and shedding of Mertk receptor in human carotid plaques: a role for oxidized polyunsaturated fatty acids? *Cardiovasc Res.* 2013;97(1):125–133.
- Ishibashi S, Goldstein JL, Brown MS, Herz J, Burns DK. Massive xanthomatosis and atherosclerosis in cholesterol-fed low density lipoprotein receptor-negative mice. *J Clin Invest.* 1994;93(5):1885–1893.
- Fredman G, et al. Targeted nanoparticles containing the proresolving peptide Ac2-26 protect against advanced atherosclerosis in hypercholesterolemic mice. *Sci Transl Med.* 2015;7(275):275ra20.
- Krishnamoorthy N, et al. Cutting edge: maresin-1 engages regulatory T cells to limit type 2 innate lymphoid cell activation and promote resolution of lung inflammation. *J Immunol.* 2015;194(3):863–867.
- Gagliani N, et al. Th17 cells transdifferentiate into regulatory T cells during resolution of inflammation. *Nature.* 2015;523(7559):221–225.
- Dietel B, Cicha I, Voskens CJ, Verhoeven E, Achenbach S, Garlachs CD. Decreased numbers of regulatory T cells are associated with human atherosclerotic lesion vulnerability and inversely correlate with infiltrated mature dendritic cells. *Atherosclerosis.* 2013;230(1):92–99.
- Foks AC, et al. Differential effects of regulatory T cells on the initiation and regression of atherosclerosis. *Atherosclerosis.* 2011;218(1):53–60.
- Fredman G, et al. An imbalance between specialized pro-resolving lipid mediators and pro-inflammatory leukotrienes promotes instability of atherosclerotic plaques. *Nat Commun.* 2016;7:12859.
- Viola JR, et al. Resolving Lipid Mediators Maresin 1 and Resolvin D2 Prevent Atheroprotection in Mice. *Circ Res.* 2016;119(9):1030–1038.
- Serhan CN, Chiang N, Van Dyke TE. Resolving inflammation: dual anti-inflammatory and pro-resolution lipid mediators. *Nat Rev Immunol.* 2008;8(5):349–361.
- Serhan CN, Krishnamoorthy S, Recchiuti A, Chiang N. Novel anti-inflammatory — pro-resolving mediators and their receptors. *Curr Top Med Chem.* 2011;11(6):629–647.
- Simiele F, et al. Transcriptional regulation of the human FPR2/ALX gene: evidence of a heritable genetic variant that impairs promoter activity. *FASEB J.* 2012;26(3):1323–1333.
- Fredman G, et al. Resolvin D1 limits 5-lipoxygenase nuclear localization and leukotriene B4 synthesis by inhibiting a calcium-activated kinase pathway. *Proc Natl Acad Sci U S A.* 2014;111(40):14530–14535.
- Bentzon JF, Otsuka F, Virmani R, Falk E. Mechanisms of plaque formation and rupture. *Circ Res.* 2014;114(12):1852–1866.
- Lin J, et al. A role of RIP3-mediated macrophage necrosis in atherosclerosis development. *Cell Rep.* 2013;3(1):200–210.
- Karunakaran D, et al. Targeting macrophage necroptosis for therapeutic and diagnostic interventions in atherosclerosis. *Sci Adv.* 2016;2(7):e1600224.
- Kojima Y, et al. CD47-blocking antibodies restore phagocytosis and prevent atherosclerosis. *Nature.* 2016;536(7614):86–90.
- Tibrewal N, et al. Autophosphorylation docking site Tyr-867 in Mer receptor tyrosine kinase allows for dissociation of multiple signaling pathways for phagocytosis of apoptotic cells and down-modulation of lipopolysaccharide-inducible NF- κ B transcriptional activation. *J Biol Chem.* 2008;283(6):3618–3627.
- Rothlin CV, Ghosh S, Zuniga EI, Oldstone MB, Lemke G. TAM receptors are pleiotropic inhibitors of the innate immune response. *Cell.* 2007;131(6):1124–1136.
- Freire-de-Lima CG, Xiao YQ, Gardai SJ, Bratton DL, Schiemann WP, Henson PM. Apoptotic cells, through transforming growth factor- β , coordinately induce anti-inflammatory and suppress pro-inflammatory eicosanoid and NO synthesis in murine macrophages. *J Biol Chem.* 2006;281(50):38376–38384.
- Li Y, Dalli J, Chiang N, Baron RM, Quintana C, Serhan CN. Plasticity of leukocytic exudates in resolving acute inflammation is regulated by MicroRNA and proresolving mediators. *Immunity.* 2013;39(5):885–898.
- Serhan CN, Savill J. Resolution of inflammation: the beginning programs the end. *Nat Immunol.* 2005;6(12):1191–1197.
- Scott RS, et al. Phagocytosis and clearance of apoptotic cells is mediated by MER. *Nature.* 2001;411(6834):207–211.
- Wu J, et al. Increased plasma levels of the soluble Mer tyrosine kinase receptor in systemic lupus erythematosus relate to disease activity and nephritis. *Arthritis Res Ther.* 2011;13(2):R62.
- Zizzo G, Guerrieri J, Dittman LM, Merrill JT, Cohen PL. Circulating levels of soluble MER in lupus reflect M2c activation of monocytes/macrophages, autoantibody specificities and disease activity. *Arthritis Res Ther.* 2013;15(6):R212.
- Qin B, et al. The association of Tyro3/Axl/Mer signaling with inflammatory response, disease activity in patients with primary Sjögren's syndrome. *Joint Bone Spine.* 2015;82(4):258–263.

SUPPLEMENTAL MATERIAL

Cai et al.

MerTK cleavage promotes plaque necrosis and defective resolution in atherosclerosis

METHODS

Study approval. For the study examining the relationship between sol-Mer and plaque necrosis, de-identified human carotid endarterectomy (CEA) specimens were provided by Dr. M.J.A.P. Daemen from the Pathology Tissue Collection (PTC) at Academic Medical Center, Amsterdam and were used in agreement with the “Code for Proper Secondary Use of Human Tissue in the Netherlands” (<http://www.fmwv.nl>). For the study examining asymptomatic versus symptomatic patients, de-identified CEA specimens were provided by Dr. Bernhard Dorweiler at the Division of Vascular Surgery, University Medical Center, Johannes-Gutenberg University, Mainz, Germany, conformed with the declaration of Helsinki and were approved for use by the university ethics review board. Informed consent was obtained from each patient. All animals were cared for according to NIH and IACUC guidelines in a barrier facility at Columbia University Medical Center, New York.

Human carotid plaque studies. For the study examining the relationship between sol-Mer with plaque necrosis, alternate carotid endarterectomy lesional cross sections were flash-frozen and extracts prepared. To detect sol-Mer, the extracts were subjected to SDS-PAGE and then immunoblotted using a monoclonal antibody (R&D systems, MAB8912) specific for the ectodomain of human MerTK. Confirming previous results using cultured macrophages (1), immunoblot of N-glycanase-treated plaque extract showed a compact band that migrated at ~60 kDa, the predicted molecular weight of

non-glycosylated sol-Mer ectodomain. Equal protein amounts were loaded per lane to normalize samples. Sol-Mer was quantified by densitometric ratio analysis using b-actin (Cell Signaling Technology, 5125) as the loading control. Flanking sections were fixed and embedded for histologic morphometric analysis. Necrotic areas were defined as acellular areas in the intima beneath the fibrous cap and quantified using ImageJ as percent necrosis based on total lesion area. For the study examining asymptomatic versus symptomatic patients, specimens were classified as either asymptomatic or symptomatic, *i.e.*, transient ischemic attack or stroke within the past 6 months, as determined by preoperative assessment by a consultant neurologist. After retrieval in the operating room the excised plaques were rinsed in physiologic saline, immediately snap frozen in liquid nitrogen, and subsequently transferred to -80°C for storage. Additionally, 5 ml of heparinized blood were obtained from each patient at the time of surgery, and the plasma was stored at -20°C. To assay sol-Mer in these samples, the specimens were cut into small pieces, homogenized, and lysed in 4x Laemmli sample buffer. Protein concentration was assayed by a reducing agent compatible protein assay kit (Thermo Scientific, Prod#23250). Equal protein was loaded on SDS-PAGE gel, and sol-Mer was detected by immunoblotting.

Animals and diets. C57BL/6J (stock #000664) and *Ldlr*^{-/-} (stock #002207) mice on the C57BL/6J background were purchased from Jackson Laboratory. *Mertk*^{CR} mice on the C57BL6/J were previously described (2). For the atherosclerosis studies, bone marrow cells from *Mertk*^{CR} mice and age-matched and sex-matched wild-type (WT) littermate control mice were transplanted into *Ldlr*^{-/-} male mice as previously described (3, 4). Briefly, *Ldlr*^{-/-} mice were irradiated using a cesium gamma source at a dose of

1000 rads. After 5 h, bone marrow from the femurs of either WT or *Mertk^{CR}* mice was injected i.v. into irradiated *Ldlr^{-/-}* mice using 5×10^6 cells per mouse. Six weeks after bone marrow transplantation, the mice were started on a Western-type diet (WD; Harlan Teklad, TD88137) and continued for 16 weeks to allow the development of advanced atherosclerosis.

Atherosclerotic lesional analyses. After 16 weeks of WD feeding, mice were fasted overnight and then sacrificed using isoflurane. Body weights were measured and blood was collected by cardiac puncture. The heart, with aortic root attached, was harvested, embedded in OCT media and frozen on dry ice. Sections of the aortic root were prepared using a cryomicrotome and then stained with hematoxylin and eosin (H&E). Six sections per mouse, spaced 30 μm apart starting from the base of the aortic root, were quantified for total lesion area and necrotic area as described previously (5). Briefly, the intimal region containing lesions is demarcated and quantified using ImagePro Plus by a person blinded to the experimental groups. Acellular areas that were $\geq 3000 \text{ mm}^2$ were marked and quantified as necrotic areas. To assess lesional cap thickness, sections were stained with collagen using picosirius red (PolySciences, #24901) as per the manufacturer's instructions. As described previously (4), fibrous cap thickness was assessed by averaging the thickness in micrometers of the cap in three separate regions of the lesions, *i.e.*, one measurement for each of the shoulder regions and one measurement in the middle of the lesion, and then expressed as arbitrary unit (AU) of cap thickness/ lesion area. For lesional *Col1a1* mRNA assay, lesional cross sections were extracted with RLT lysis buffer (Qiagen) to obtain RNA, which was then quantified for *Col1a1* mRNA using RT-qPCR with the following primers: forward 5'-

GCTCCTCTTAGGGGCCACT-3', reverse 5'-CCACGTCTCACCATTGGGG-3'. Plasma cholesterol and triglycerides were measured using the Cholesterol E kit (Wako, 439-17501) and L-type Triglyceride M kit (Wako, 465-09791 and 461-09891) respectively. Fasting blood glucose was measured using glucose test strips and a glucometer.

In vitro efferocytosis assay. Bone marrow-derived macrophages were incubated with PKH green-labeled apoptotic Jurkat cells were added to the macrophages at a ratio of 3:1 or 5:1 (apoptotic cells:macrophages) for 45 mins and then fixed and analyzed by fluorescence microscopy. The percentage of total BMDMs with internalized labeled apoptotic cells (efferocytosis) was quantified by analysis of fluorescence microscopy images. In Supplemental Figure 1E, some of the cells were co-incubated with recombinant mouse Mer-Fc chimera protein (rMer-Fc; R&D Systems #591-MR).

In situ efferocytosis assay. Following established procedures described previously (6), efferocytosis was determined *in situ* by counting the number of free versus macrophage-associated apoptotic cells in individual lesion sections. Frozen aortic root sections were fixed with cold acetone for 5 mins. After washing with PBS, sections were stained with terminal deoxynucleotidyl transferase dUTP nick end labeling (TUNEL, Roche, 12156792910) to identify apoptotic cells, followed by anti-F4/80 immunostaining to label lesional macrophages. Slides were then mounted with DAPI-containing mounting solution. As a measure of defective efferocytosis, we counted the number of free versus macrophage-associated apoptotic cells in individual lesional sections. *Free* apoptotic cells were defined as TUNEL⁺ cells that exhibited nuclear condensation, loss of antibody F4/80 reactivity, and were not in contact with neighboring macrophages.

Macrophage-associated apoptotic cells were defined as cells with TUNEL+ nuclei surrounded by or in contact with neighboring F4/80⁺ macrophages.

Mouse aortic sol-Mer assay. After 16 weeks of WD feeding, mice were sacrificed, and aortic arch, brachiocephalic artery (BCA), descending aorta up to the bifurcation of the renal arteries (referred to as "aorta") were harvested and snap frozen in liquid nitrogen. Aortic tissue was then homogenized and lysed with 4x Laemmli sample buffer. The protein concentration was measured using a protein assay kit (Thermo Scientific, Prod#23250). Equal amounts of protein were subjected to SDS polyacrylamide gel electrophoresis and transferred to nitrocellulose. Sol-Mer was detected with a goat anti-MerTK antibody that is specific for the ectodomain of mouse MerTK (R&D system, AF591). For the quantification of sol-Mer released into macrophage culture medium, bone marrow-derived macrophages were incubated for 3 h in 500 μ L of serum-free medium containing vehicle or 50 μ g/mL oxLDL (Alfa Aesar, J65591). The media were collected, concentrated 10-fold with ultracentrifugal filters (10,000 molecular weight cut-off; Amicon, UFC501096), lysed with 4x Laemmli sample buffer, and subjected to SDS polyacrylamide gel electrophoresis and immunoblot analysis.

Assay of sol-Mer in the media of cultured macrophages. Bone marrow-derived macrophages were resuspended in 500 μ L of serum-free media and then treated as indicated in the figure legends. The media were collected, concentrated 10-fold using ultracentrifugal filters (10,000 Da molecular weight cut-off; Amicon, UFC501096), lysed with 4x Laemmli sample buffer, and subjected to SDS polyacrylamide gel electrophoresis and immunoblot analysis.

Quantification of lesional MerTK by immunofluorescence microscopy. For analysis of MerTK in human carotid lesions, carotid specimens were fixed in 4% formalin overnight, decalcified in ethylenediaminetetraacetic acid buffer (EDTA, pH 7.2) for 4 days, and embedded in paraffin blocks. Sections were cut serially at 5- μ m intervals and mounted on slides. Prior to staining, sections were deparaffinized in xylene and rehydrated in a graded series of ethanol. Sections were then placed in a pressure cooker for 10 mins in citrate-based solution (pH 6.0, Vector laboratories, H-3300) to expose antigens. After rinsing in phosphate buffered saline (PBS, pH 7.4) and blocking in serum-free protein blocking buffer (Dako, X0909), the sections were incubated with mouse anti-human MerTK (Abcam, ab52968) at 4^o C overnight, followed by incubation with Alexa fluor 594-conjugated anti-mouse secondary antibody (Thermo Scientific, A-11005) for 1 h. Slides were then mounted with DAPI-containing mounting solution (Thermo Scientific, P36935). Three imaging fields were obtained for each patient sample using a Nikon A1 confocal microscopy. In ImageJ, for each field of image, a threshold was set to reduce image background and the DAPI+ area was selected in which to measure the mean of intensity (MFI) of MerTK staining. Three fields per section for each patient were randomly chosen for imaging by confocal microscopy. In ImageJ, a threshold was set to reduce image background, using the same setting for all images. DAPI-positive areas were then analyzed for the mean of intensity (MFI) of MerTK staining within this area for each field. The MFI from the 3 fields was averaged for each patient. For mouse lesional MerTK staining, frozen sections were fixed in cold acetone for 5 mins. After washing in PBS, sections were incubated with biotin-blocking buffer (Thermo Scientific, E21390) to block endogenous biotin. Sections were then incubated with biotin-labeled anti-mouse

MerTK (R&D system, BAF591) at 4° C overnight, followed by incubation with Alexa fluor 488-conjugated streptavidin (Thermo Scientific, S11223) for 1 h. Slides were mounted with DAPI-containing mounting solution. Images of every lesion for each mouse were analyzed. Image background was reduced using the same threshold setting for each image, and then the images were analyzed the MFI of MerTK in DAPI+ areas for each lesion. The MFI of all the lesions for each mouse was averaged.

Quantification of lesional cells by immunofluorescence microscopy. The number of total cells (DAPI⁺), macrophages (F4/80⁺(Bio-Rad, MCA771G)), smooth muscle cells (SMC, α -actin⁺(Sigma, C6198)) and dendritic cells (DC, MHC-II⁺CD11c⁺(MHC- II: eBioscience, 13-5321-81; CD11c:BD Bioscience, 561044)) were quantified in immunostained aortic root section images using immunofluorescence microscopy followed by analysis using ImageJ software. The percentage of lesional cell subtypes was defined as the number of cells positive for the individual marker relative to the total number of DAPI⁺ cells within the lesion. In separate sections, the number of total T cells (CD3⁺(Abcam, ab16669)), CD4⁺T cells (CD3⁺ CD4⁺(CD4: eBioscience, 14-0041-82)) and Treg cells (Foxp3⁺CD3⁺(Foxp3: eBioscience, 14-5773-82)) were counted. These were quantified as the number of positive cells relative to total cells per section including adventitia.

Identification and quantification of lipid mediators by LC-MS/MS. Aortas were collected, immediately placed in cold methanol containing deuterium-labeled standards (d₅-RvD2, d₅-LXA₄, d₄-LTB₄, d₅-LTC₄, d₅-LTD₄, d₄-PGE₂, d₈-5-HETE), and subjected to solid-phase (C₁₈) extraction as described previously (7). Methyl formate and methanol fractions were collected, the solvents were evaporated with N₂ gas, and samples were

resuspended in methanol:water (50:50) immediately prior to automated injection on a HPLC (Shimadzu) coupled to a Qtrap5500 mass spectrometer (AB Sciex). The instrument was operated in positive ion mode (cysteinyl leukotrienes) or negative ion mode (all others) and lipid mediators were identified using established scheduled multiple reaction monitoring (MRM) transitions (8). Quantification was carried out based on recovery of internal deuterium labeled standards and external calibration curves for each individual lipid mediator using authentic standards (Cayman Chemical). To generate an index of the SPM, we combined RvD1-6, 17R-RvD1, Mar1, Mar2, PD1, 10S,17S-diHDHA, 15R-LXA₄, LXB₄, RvE2 and RvE3 (see Figure 3D), while the total 5-LOX-derived SPMs displayed in Figure 3E include RvD1-6, 17R-RvD1, LXB₄, 15R-LXA₄, and RvE2, divided by all leukotrienes (LTB₄, LTC₄, LTD₄, LTE₄). Values for each individual lipid mediator are given in Table 1.

RvD1 treatment of Ldlr^{-/-} mice. 8-10 week-old male *Ldlr^{-/-}* mice were placed on the WD for a total of 17 weeks. At the 12-week time point, the mice were injected i.p. 3 times per week with 500 µl of sterile PBS (vehicle control) or RvD1 (100 ng/mouse, Cayman Chemical, 10012554) for an additional 5 weeks while still on the WD. Cross-sections of murine aortic root lesion were stained with a biotinylated anti-MerTK (R&D system, BAF591) antibody at 4°C overnight. Slides were gently washed with PBS, and a streptavidin secondary antibody was then added to the slides for 2 h at room temperature. The sections were counterstained with Hoechst to identify nuclei, viewed on a Nikon A1 confocal microscope, and analyzed using ImageJ software.

1. Sather,S., Kenyon,K.D., Lefkowitz,J.B., Liang,X., Varnum,B.C., Henson,P.M., and Graham,D.K. 2007. A soluble form of the Mer receptor tyrosine kinase inhibits macrophage clearance of apoptotic cells and platelet aggregation. *Blood* **109**:1026-1033.
2. Cai,B., Thorp,E.B., Doran,A.C., Subramanian,M., Sansbury,B.E., Lin,C.S., Spite,M., Fredman,G., and Tabas,I. 2016. MerTK cleavage limits proresolving mediator biosynthesis and exacerbates tissue inflammation. *Proc. Natl. Acad. Sci. U. S. A.* **113**:6526-6531.
3. Wang,Y., Wang,G.Z., Rabinovitch,P.S., and Tabas,I. 2014. Macrophage mitochondrial oxidative stress promotes atherosclerosis and nuclear factor-kappaB-mediated inflammation in macrophages. *Circ. Res.* **114**:421-433.
4. Fredman,G., Kamaly,N., Spolitu,S., Milton,J., Ghorpade,D., Chiasson,R., Kuriakose,G., Milton,J., Perretti,M., Farokhzad,O.C. et al 2015. Targeted nanoparticles containing the pro-resolving peptide Ac2-26 protect against advanced atherosclerosis in hypercholesterolemic mice. *Sci. Transl. Med.* **7**:275ra20.
5. Subramanian,M., Thorp,E.B., and Tabas,I. 2014. Identification of a non-growth factor role for GM-CSF in advanced atherosclerosis: promotion of macrophage apoptosis and plaque necrosis through IL-23 signaling. *Circ. Res.* **116**:e13-e24.
6. Thorp,E., Cui,D., Schrijvers,D.M., Kuriakose,G., and Tabas,I. 2008. MERTK receptor mutation reduces efferocytosis efficiency and promotes apoptotic cell accumulation and plaque necrosis in atherosclerotic lesions of *ApoE*^{-/-} mice. *Arterioscler. Thromb. Vasc. Biol.* **28**:1421-1428.
7. Fredman,G., Hellmann,J., Proto,J.D., Kuriakose,G., Colas,R.A., Dorweiler,B., Connolly,E.S., Solomon,R., Jones,D.M., Heyer,E.J. et al 2016. An imbalance between specialized pro-resolving lipid mediators and pro-inflammatory leukotrienes promotes instability of atherosclerotic plaques. *Nat. Commun.* **7**:12859.
8. Colas,R.A., Shinohara,M., Dalli,J., Chiang,N., and Serhan,C.N. 2014. Identification and signature profiles for pro-resolving and inflammatory lipid mediators in human tissue. *Am. J. Physiol Cell Physiol* **307**:C39-C54.

Supplemental Table 1 SPMs and pro-inflammatory lipid mediators in aortic extracts from WT \otimes *Ldlr*^{-/-} and *Mertk*^{CR} \otimes *Ldlr*^{-/-} BMT mice.

Compound	WT \otimes <i>Ldlr</i> ^{-/-}			<i>Mertk</i> ^{CR} \otimes <i>Ldlr</i> ^{-/-}			P
	(pg/mg)	SEM (\pm)	n	(pg/mg)	SEM (+/-)	n	
DHA Metabolome							
RvD1	43.8	8.7	5	65.1	19.6	8	0.431
17R-RvD1	292.2	63.5	8	690.8	168.9	9	0.053
RvD2	71.8	19.5	7	186.5	37.1	8	0.021
RvD3	3.2	0.5	2	12.5	3.3	6	0.181
17R-RvD3	-	-	-	-	-	-	-
RvD5	8.3	1.8	8	3.6	0.6	9	0.018
RvD6	2.4	0.6	8	4.3	0.7	9	0.056
Mar1	58.7	11.9	8	58.6	7.6	9	0.994
Mar2	22.9	13.7	7	58.0	27.4	8	0.294
PD1	160.3	32.3	7	247.9	28.6	9	0.062
17R-PD1	-	-	-	-	-	-	-
10S,17S-diHDHA	9.2	-	1	3.7	0.8	7	-
21-HDHA	0.3	0.1	8	0.1	0.0	9	0.005
17-HDHA	41.1	10.7	8	32.1	4.3	9	0.429
14-HDHA	222.9	48.7	8	183.4	23.7	9	0.461
13-HDHA	35.9	5.5	8	32.1	4.2	9	0.589
7-HDHA	11.1	1.9	8	12.9	2.0	9	0.522
4-HDHA	26.6	4.5	8	23.6	3.2	9	0.582
AA Metabolome							
LXA ₄	-	-	-	-	-	-	-

15 <i>R</i> -LXA ₄	12.8	2.6	8	15.1	1.7	9	0.469
LXB ₄	23.9	4.7	8	22.7	3.3	9	0.841
15 <i>R</i> -LXB ₄	-	-	-	-	-	-	-
LTB ₄	163.5	26.6	8	203.0	34.8	9	0.390
6- <i>trans</i> LTB ₄	79.5	10.2	8	130.9	17.7	9	0.028
6- <i>trans</i> ,12- <i>epi</i> LTB ₄	69.4	13.5	8	119.6	20.1	9	0.062
LTC ₄	9.1	2.1	7	4.8	1.0	9	0.070
LTD ₄	3.5	1.0	7	2.9	0.6	9	0.659
LTE ₄	2.2	0.7	7	1.7	0.5	9	0.586
PGE ₂	671.0	137.2	8	803.1	129.5	9	0.495
PGD ₂	565.4	90.6	8	629.5	67.9	9	0.574
PGF _{2α}	168.9	33.9	8	165.1	22.2	9	0.924
TxB ₂	1009.7	150.1	8	858.3	93.7	9	0.394
5 <i>S</i> ,6 <i>R</i> -diHETE	54.8	10.4	8	68.6	12.3	9	0.411
5 <i>S</i> ,15 <i>S</i> -diHETE	81.5	15.1	8	90.2	15.8	9	0.700
15-HETE	466.0	84.8	8	433.5	50.6	9	0.740
12-HETE	5213.5	825.5	8	3722.8	461.3	9	0.125
11-HETE	587.1	93.9	8	589.6	72.7	9	0.983
5-HETE	77.5	15.1	8	69.9	9.8	9	0.672
12-HHT	278.9	48.1	8	267.0	27.7	9	0.829
EPA Metabolome							
RvE1	-	-	-	-	-	-	-
RvE2	303.8	62.6	8	412.7	38.6	9	0.149
5 <i>S</i> ,15 <i>S</i> -diHEPE	21.7	4.5	8	16.6	1.4	8	0.299
RvE3	298.2	50.6	8	504.6	72.4	9	0.038
LXA ₅	-	-	-	-	-	-	-
LXB ₅	-	-	-	-	-	-	-

18-HEPE	12.2	2.1	8	11.5	1.4	9	0.794
15-HEPE	29.2	7.8	8	29.1	3.9	9	0.986
12-HEPE	1019.3	164.6	8	734.8	92.0	9	0.141
11-HEPE	24.9	3.9	8	24.3	2.7	9	0.909
5-HEPE	9.4	1.4	8	9.8	1.1	9	0.799

Compounds are displayed as pg/mg of aortic protein and expressed as mean \pm SEM. The limit of detection is \sim 0.1 pg; values below this limit are indicated by "-".

SUPPLEMENTAL FIGURE LEGENDS

Supplemental Figure 1. Analyses of sol-Mer and macrophage content of human

carotid endarterectomy specimens. (A) Representative sol-Mer immunoblots and H&E-stained cross-sections of the human carotid endarterectomy specimens from 5 of the patients (P) analyzed in Figure 1A. NC, necrotic core (bar, 80 μ m). The sol-Mer: β -actin densitometric ratio and % lesional necrosis are shown below each lane of the immunoblot. **(B)** Sol-Mer in plasma from asymptomatic and symptomatic patients was assayed by ELISA (n=6-8 per group. *P<0.05). **(C)** Bone marrow-derived macrophages were incubated for 45 min with PKH green-labeled apoptotic Jurkat T cells at a ratio of 1:5 in the presence of increasing doses of rMer-Fc. The percent of macrophages with internalized labeled apoptotic cells (efferocytosis) was quantified by analysis of fluorescence microscopy images (n=3 for each treatment, *, P<0.05, **P<0.01). **(D)** CD68+ macrophages were quantified in lesional sections from the asymptomatic and symptomatic subjects described in Figure 1B-C (n=6-8 per group). n.s, no significance. **(B-D)** Two-tailed Student's t test was used to evaluate significance.

Supplemental Figure 2. OxLDL- induced MerTK cleavage depends on ADAM17

activity and is absent in *Mertk*^{CR} macrophages. (A) Bone marrow-derived macrophages (BMDMs) were pre-treated with 10 μ M TAPI-0 for 30 mins after which either vehicle control or 50 μ g/ml oxLDL was added to the medium. After 3 h, sol-Mer from culture media and β -actin from cell lysates were detected by immunoblot. **(B)** Either WT or *Mertk*^{CR} BMDMs were treated with oxLDL for 3 h, followed by immunoblot of sol-Mer and β -actin. **(C)** After oxLDL treatment, MerTK MFI on BMDMs was

quantified by immunofluorescence microscopy (n=3 replicates for each treatment, *P<0.05) (D) BMDMs were incubated with 50 mg/ml oxLDL. After 3 h, PKH-green-labeled apoptotic Jurkat cells (AC) were added to the macrophages at a ratio of 3:1 (apoptotic cells:macrophages) for 45 mins. The percent of total BMDMs with internalized labeled apoptotic cells (efferocytosis) was quantified by analysis of fluorescence microscopy images (n=3 replicates for each treatment. *P<0.05). (C-D) Two-tailed Student's t test was used to evaluate significance.

Supplemental Figure 3. Body weight, blood glucose and plasma lipids are similar between 16-wk WD-fed WT \otimes *Ldlr*^{-/-} and *Mertk*^{CR} \otimes *Ldlr*^{-/-} mice. (A-D) Body weight, blood glucose after 5-h food withdrawal, and plasma cholesterol and triglycerides after an overnight fast in 16-week WD-fed WT \otimes *Ldlr*^{-/-} or *Mertk*^{CR} \otimes *Ldlr*^{-/-} mice (n=10 per group). n.s, no significance. Two-tailed Student's t test was used to evaluate significance.

Supplemental Figure 4. Blood leukocytes numbers are similar between 16-wk WD-fed WT \otimes *Ldlr*^{-/-} and *Mertk*^{CR} \otimes *Ldlr*^{-/-} mice. (A-D) Circulating total white blood cells, neutrophils, monocytes, and platelets in 16-week WD-fed WT \otimes *Ldlr*^{-/-} or *Mertk*^{CR} \otimes *Ldlr*^{-/-} mice (n=10 per group). n.s, no significance. Two-tailed Student's t test was used to evaluate significance.

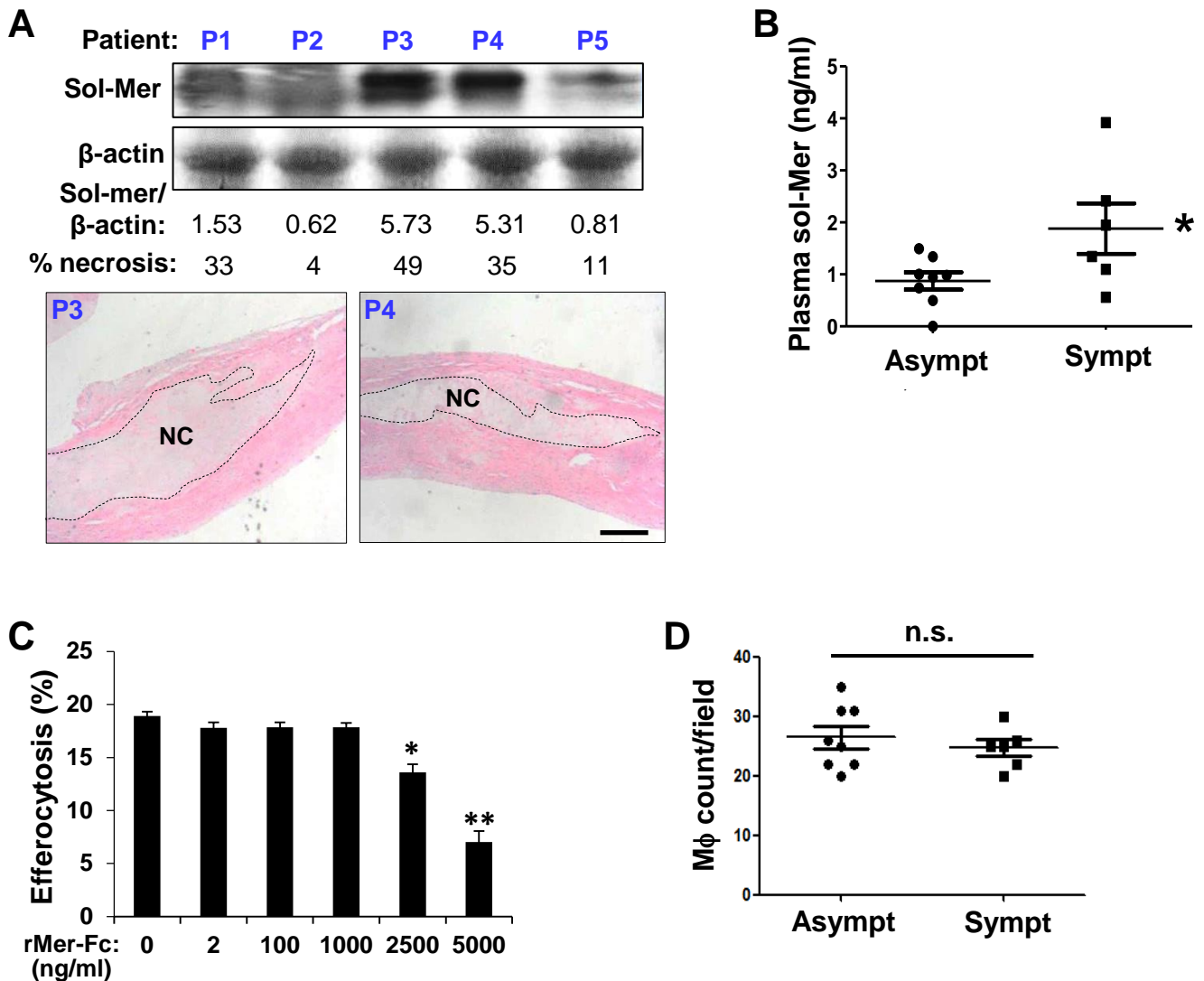
Supplemental Figure 5. Analysis of total lesion area and lesional cell populations in 16-wk WD-fed BMT mice. (A-B) Aortic root sections from 16-week WD-fed WT \otimes *Ldlr*^{-/-} or *Mertk*^{CR} \otimes *Ldlr*^{-/-} mice were quantified for total lesion area and total cell number (DAPI⁺ cells) (n=10 per group). n.s, no significance. (C) The sections were probed for

the indicated cell types using immunofluorescence microscopy, and cell numbers per total lesional cells, per total cells in aortic root cross sections, or as a ratio were quantified using ImageJ. The antibodies used were against F4/80 and CD206 (macrophages), α actin (smooth muscle cells), CD3 (total T cells), CD4 (CD4⁺ T cells), and MHC-II and CD11c (dendritic cells; DC). n=10 per group. n.s, no significance. (A-C) Two-tailed Student's t test was used to evaluate significance.

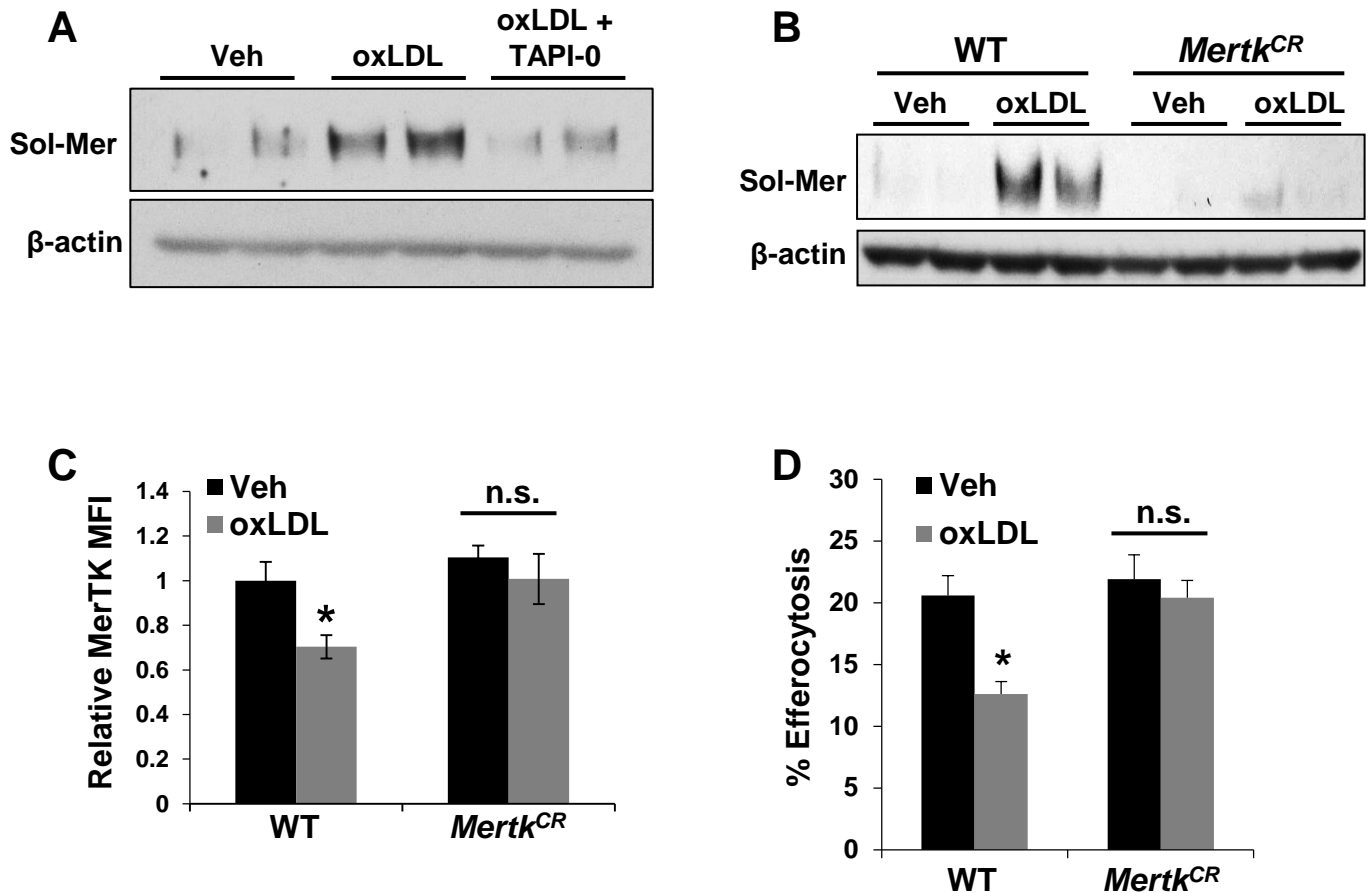
Supplemental Figure 6. Plasma TGF β 1, IL10 and FPR2 expression in lesional cells are increased 16-wk WD-fed *Mertk*^{CR} ® *Ldlr*^{-/-} mice. Wild-type (WT) ® *Ldlr*^{-/-} or *Mertk*^{CR} ® *Ldlr*^{-/-} BMT mice were placed on the WD for 16 wks. (A) Aortic root sections were stained with picosirius red. Images illustrate the strategy used to measure cap thickness (bar, 40 μ m). **(B)** Plasma TGF β 1 and IL-10 were assayed by ELISA (n=8-9 for per group. *, P<0.05). **(C)** Aortic root lesions were immunostained for ALX/FPR2 (red) and counterstained with the nuclear dye DAPI (blue) (bar, 30 mm). The ALX/FPR2 mean fluorescence intensity (MFI) per lesion section was quantified by image analysis of cross-sections and expressed relative to the WT value (n=8-9 per group. *P<0.05). (B-C) Two-tailed Student's t test was used to evaluate significance.

Supplemental Figure 7. RvD1 prevents LPS-induced MerTK cleavage and increases MerTK intensity in atherosclerotic lesions. (A-B) Macrophages were incubated with 10 nM RvD1 for 5 h and then with 50 ng/mL LPS for 2 h. The media were assayed for sol-Mer by immunoblot. The attached cells were immunostained for MerTK under non-permeabilizing conditions, and then cell-surface MerTK was quantified by fluorescence microscopy (n=3 replicates for each treatment, **P<0.01). **(C)**

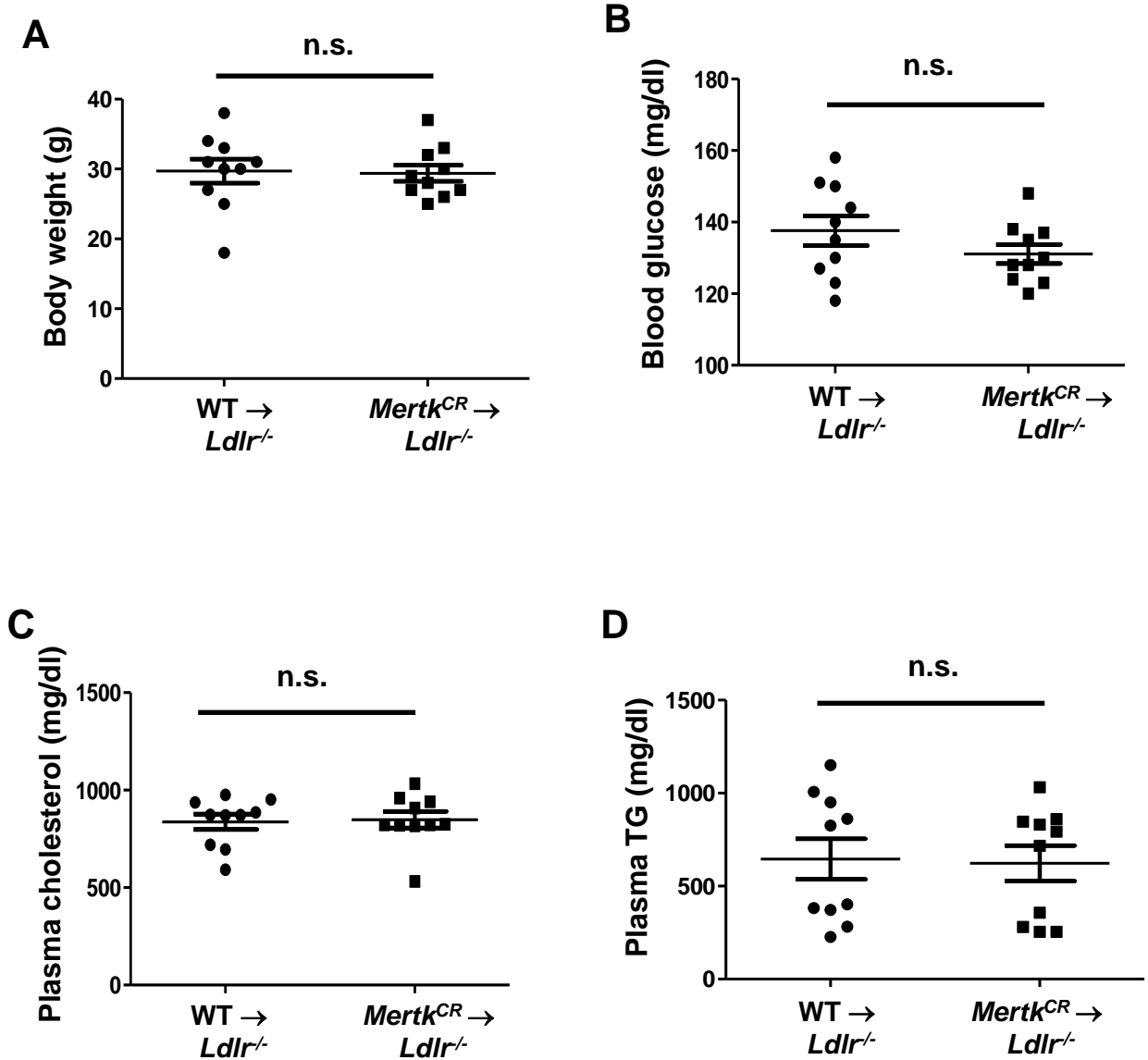
Ldlr^{-/-} mice were fed the WD for 12 wks and then treated with control (Veh) or 100 ng RvD1/mouse (3x/wk i.p.) for 5 additional wks, with the mice continued on WD. Aortic root lesions were immunostained for MerTK (red) and counterstained with the nuclear dye DAPI (blue) (bar, 50 mm). The MerTK mean fluorescence intensity (MFI) per lesion section was quantified by image analysis of cross-sections and expressed relative to the Veh value (n=8-10 per group). *P<0.05 (B-C) Two-tailed Student's t test was used to evaluate significance.



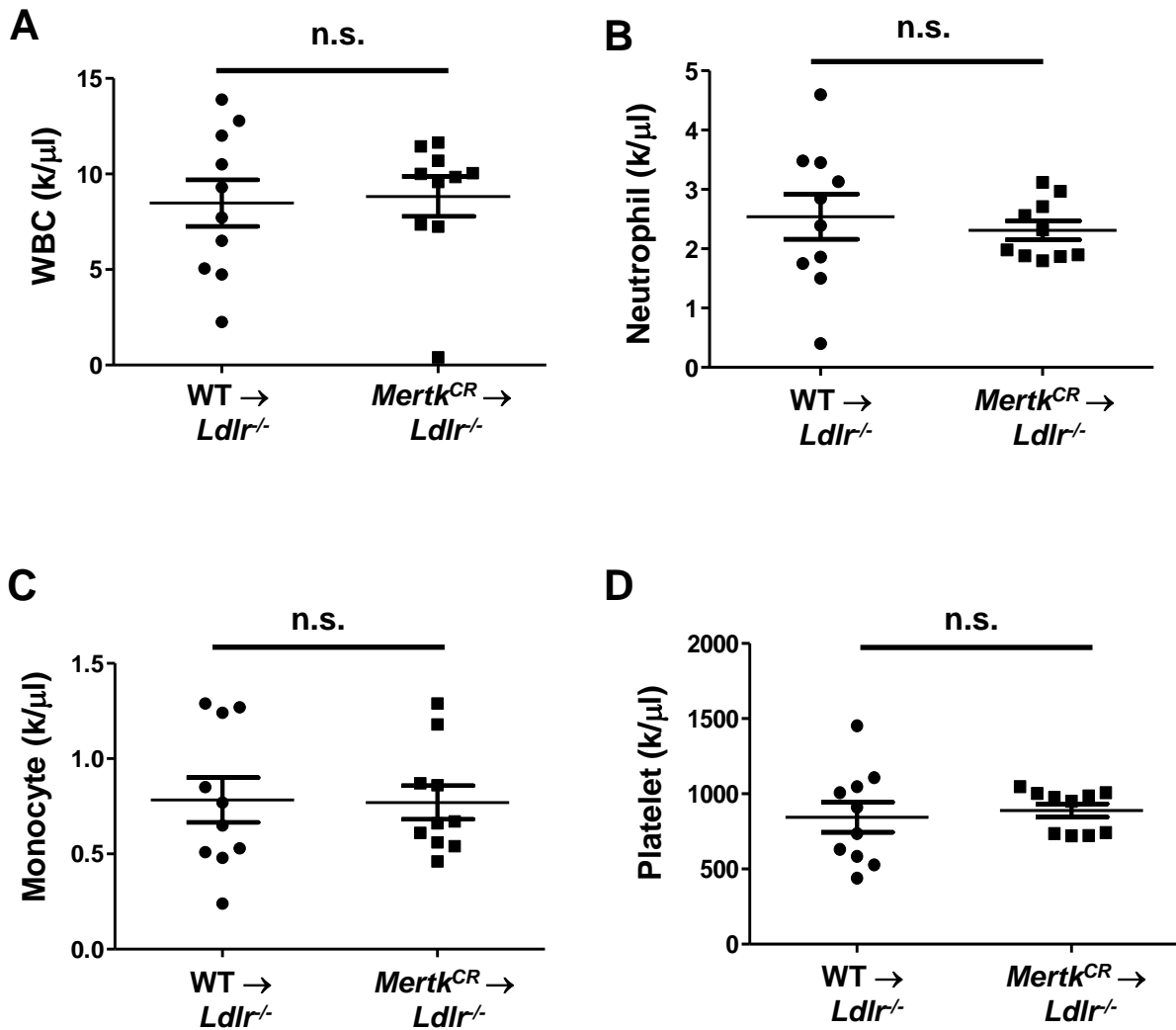
Supplemental Figure 1. Analyses of sol-Mer and macrophage content of human carotid endarterectomy specimens. (A) Representative sol-Mer immunoblots and H&E-stained cross-sections of the human carotid endarterectomy specimens from 5 of the patients (P) analyzed in Figure 1A. NC, necrotic core (bar, 80 μ m). The sol-Mer: β -actin densitometric ratio and % lesional necrosis are shown below each lane of the immunoblot. (B) Sol-Mer in plasma from asymptomatic and symptomatic patients was assayed by ELISA (n=6-8 per group. *P<0.05). (C) Bone marrow-derived macrophages were incubated for 45 min with PKH green-labeled apoptotic Jurkat T cells at a ratio of 1:5 in the presence of increasing doses of rMer-Fc. The percent of macrophages with internalized labeled apoptotic cells (efferocytosis) was quantified by analysis of fluorescence microscopy images (n=3 for each treatment, *, P<0.05, **P<0.01). (D) CD68+ macrophages were quantified in lesional sections from the asymptomatic and symptomatic subjects described in Figure 1B-C (n=6-8 per group). n.s, no significance. (B-D) Two-tailed Student's t test was used to evaluate significance.



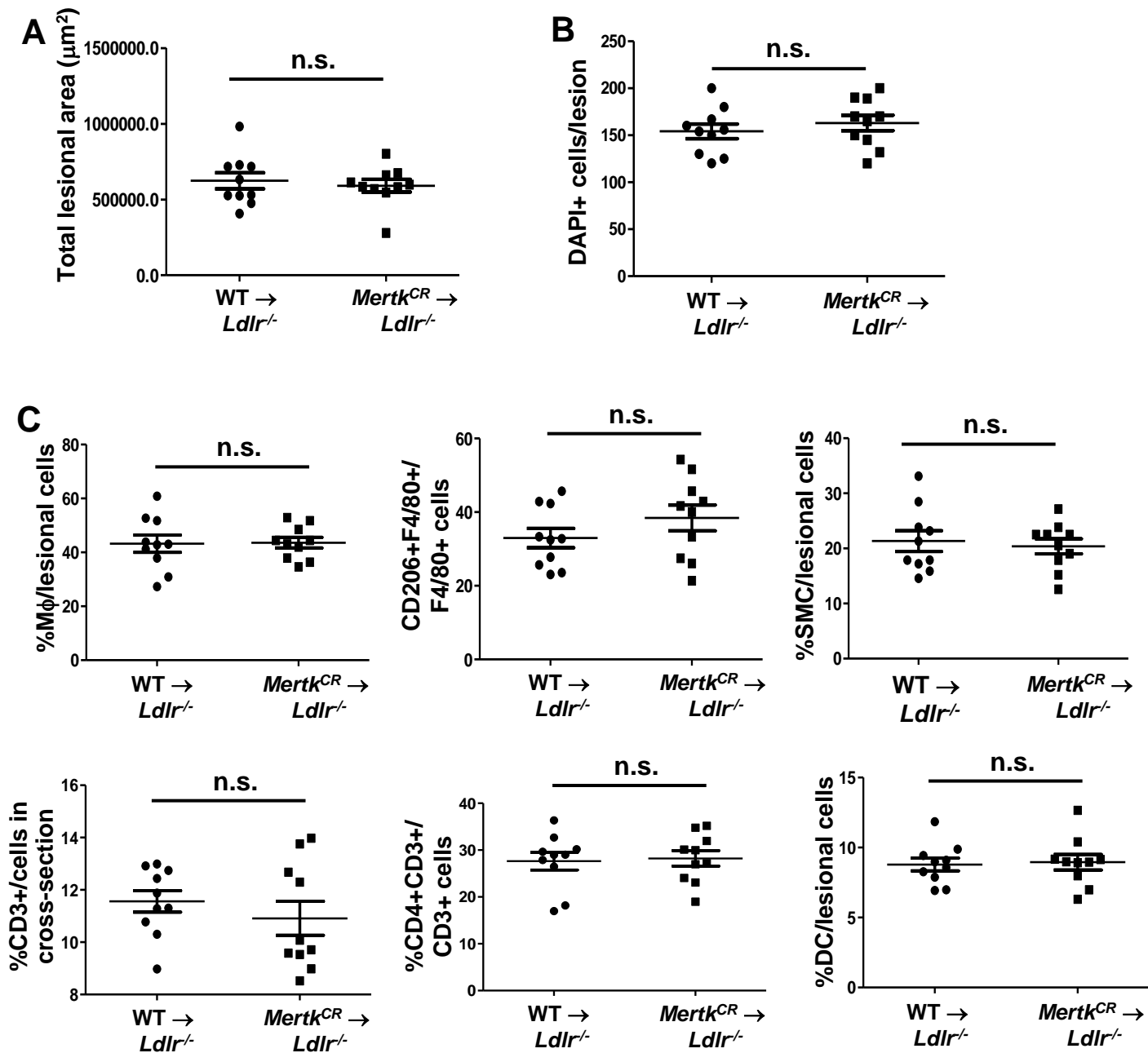
Supplemental Figure 2. OxLDL- induced MerTK cleavage depends on ADAM17 activity and is absent in *Mertk*^{CR} macrophages. (A) Bone marrow-derived macrophages (BMDMs) were pre-treated with 10 μ m TAPI-0 for 30 mins after which either vehicle control or 50 μ g/ml oxLDL was added to the medium. After 3 h, sol-Mer from culture media and β -actin from cell lysates were detected by immunoblot. (B) Either WT or *Mertk*^{CR} BMDMs were treated with oxLDL for 3 h, followed by immunoblot of sol-Mer and β -actin. (C) After oxLDL treatment, MerTK MFI on BMDMs was quantified by immunofluorescence microscopy (n=3 replicates for each treatment, *P<0.05) (D) BMDMs were incubated with 50 μ g/ml oxLDL. After 3 h, PKH-green-labeled apoptotic Jurkat cells (AC) were added to the macrophages at a ratio of 3:1 (apoptotic cells:macrophages) for 45 mins. The percent of total BMDMs with internalized labeled apoptotic cells (efferocytosis) was quantified by analysis of fluorescence microscopy images (n=3 replicates for each treatment. *P<0.05). (C-D) Two-tailed Student's t test was used to evaluate significance.



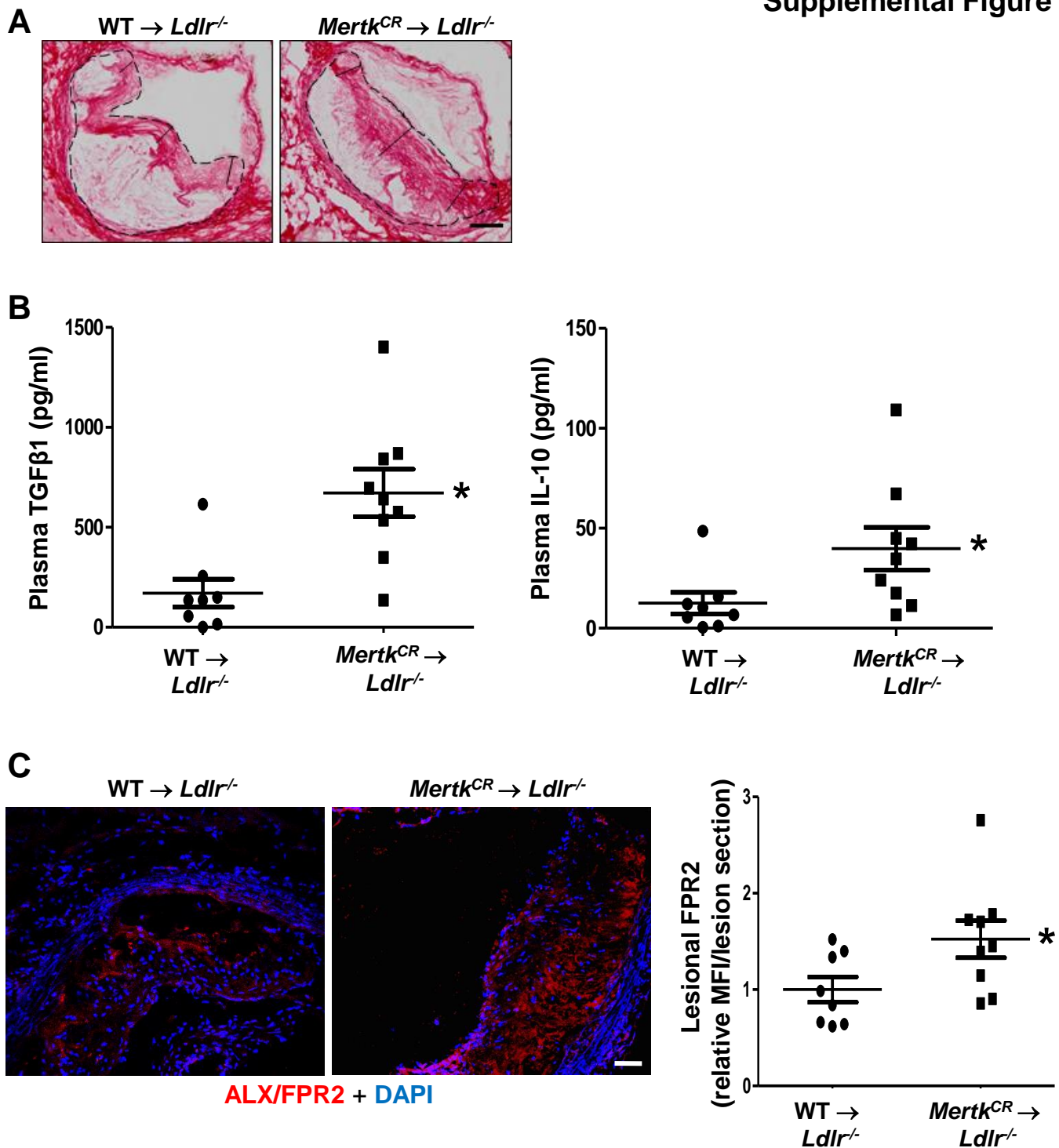
Supplemental Figure 3. Body weight, blood glucose and plasma lipids are similar between 16-wk WD-fed WT \rightarrow *Ldlr*^{-/-} and *Mertk*^{CR} \rightarrow *Ldlr*^{-/-} mice. (A-D) Body weight, blood glucose after 5-h food withdrawal, and plasma cholesterol and triglycerides after an overnight fast in 16-week WD-fed WT \rightarrow *Ldlr*^{-/-} or *Mertk*^{CR} \rightarrow *Ldlr*^{-/-} mice (n=10 per group). n.s., no significance. Two-tailed Student's t test was used to evaluate significance.



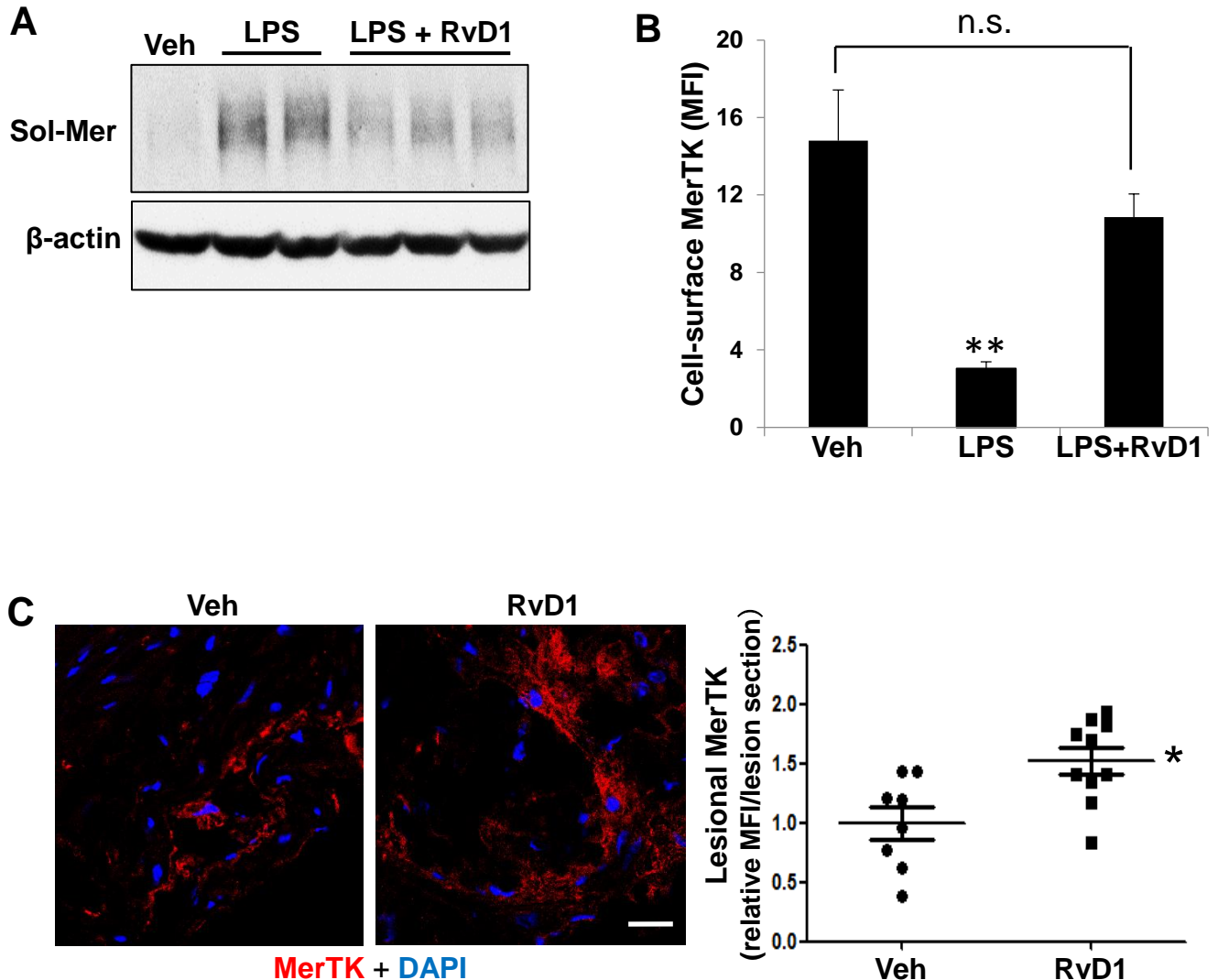
Supplemental Figure 4. Blood leukocytes numbers are similar between 16-wk WD-fed WT \rightarrow *Ldlr*^{-/-} and *Mertk*^{CR} \rightarrow *Ldlr*^{-/-} mice. (A-D) Circulating total white blood cells, neutrophils, monocytes, and platelets in 16-week WD-fed WT \rightarrow *Ldlr*^{-/-} or *Mertk*^{CR} \rightarrow *Ldlr*^{-/-} mice (n=10 per group). n.s., no significance. Two-tailed Student's t test was used to evaluate significance.



Supplemental Figure 5. Analysis of total lesion area and lesional cell populations in 16-wk WD-fed BMT mice. (A-B) Aortic root sections from 16-week WD-fed WT \rightarrow *Ldlr*^{-/-} or *Mertk*^{CR} \rightarrow *Ldlr*^{-/-} mice were quantified for total lesion area and total cell number (DAPI⁺ cells) (n=10 per group). n.s, no significance. (C) The sections were probed for the indicated cell types using immunofluorescence microscopy, and cell numbers per total lesional cells, per total cells in aortic root cross sections, or as a ratio were quantified using ImageJ. The antibodies used were against F4/80 and CD206 (macrophages), α actin (smooth muscle cells), CD3 (total T cells), CD4 (CD4⁺ T cells), and MHC-II and CD11c (dendritic cells; DC). n=10 per group. n.s, no significance. (A-C) Two-tailed Student's t test was used to evaluate significance.



Supplemental Figure 6. Plasma TGFβ1, IL10 and FPR2 expression in lesional cells are increased 16-wk WD-fed *Mertk*^{CR} → *Ldlr*^{-/-} mice. Wild-type (WT) → *Ldlr*^{-/-} or *Mertk*^{CR} → *Ldlr*^{-/-} BMT mice were placed on the WD for 16 wks. (A) Aortic root sections were stained with picrosirius red. Images illustrate the strategy used to measure cap thickness (bar, 40 μm). (B) Plasma TGFβ1 and IL-10 were assayed by ELISA (n=8-9 for per group. *, P<0.05). (C) Aortic root lesions were immunostained for ALX/FPR2 (red) and counterstained with the nuclear dye DAPI (blue) (bar, 30 μm). The ALX/FPR2 mean fluorescence intensity (MFI) per lesion section was quantified by image analysis of cross-sections and expressed relative to the WT value (n=8-9 per group. *P<0.05). (B-C) Two-tailed Student's t test was used to evaluate significance.



Supplemental Figure 7. RvD1 prevents LPS-induced MerTK cleavage and increases MerTK intensity in atherosclerotic lesions. (A-B) Macrophages were incubated with 10 nM RvD1 for 5 h and then with 50 ng/mL LPS for 2 h. The media were assayed for sol-Mer by immunoblot. The attached cells were immunostained for MerTK under non-permeabilizing conditions, and then cell-surface MerTK was quantified by fluorescence microscopy (n=3 replicates for each treatment, **P<0.01). (C) *Ldlr*^{-/-} mice were fed the WD for 12 wks and then treated with control (Veh) or 100 ng RvD1/mouse (3x/wk i.p.) for 5 additional wks, with the mice continued on WD. Aortic root lesions were immunostained for MerTK (red) and counterstained with the nuclear dye DAPI (blue) (bar, 50 μ m). The MerTK mean fluorescence intensity (MFI) per lesion section was quantified by image analysis of cross-sections and expressed relative to the Veh value (n=8-10 per group). *P<0.05 (B-C) Two-tailed Student's t test was used to evaluate significance.